*Inorg. Chem.* **2002**, *41*, 4478–4487


# EPR Spectra from "EPR-Silent" Species: High-Frequency and High-Field EPR Spectroscopy of Pseudotetrahedral Complexes of Nickel(II)

**J. Krzystek,[§] Ju-Hyun Park,[#] Mark W. Meisel,[#] Michael A. Hitchman,[‡] Horst Stratemeier,[‡] Louis-Claude Brunel,[§] and Joshua Telser*,[†]**

*Center for Interdisciplinary Magnetic Resonance, National High Magnetic Field Laboratory, Florida State University, Tallahassee, Florida 32310, Department of Physics and Center for Condensed Matter Sciences, University of Florida, Gainesville, Florida 32611-8440, Department of Chemistry, University of Tasmania, Hobart, Tasmania, Australia, and Chemistry Program, Roosevelt University, Chicago, Illinois 60605-1394*

Received March 12, 2002

High-frequency and high-field electron paramagnetic resonance (HFEPR) spectroscopy (using frequencies of ∼90–550 GHz and fields up to ∼15 T) has been used to probe the non-Kramers, $S = 1$, $Ni^{2+}$ ion in a series of pseudotetrahedral complexes of general formula $NiL_2X_2$, where L = $PPh_3$ (Ph = phenyl) and X = Cl, Br, and I. Analysis based on full-matrix solutions to the spin Hamiltonian for an $S = 1$ system gave zero-field splitting parameters: $D = +13.20(5)$ cm$^{-1}$, $|E| = 1.85(5)$ cm$^{-1}$, $g_x = g_y = g_z = 2.20(5)$ for $Ni(PPh_3)_2Cl_2$. These values are in good agreement with those obtained by powder magnetic susceptibility and field-dependent magnetization measurements and with earlier, single-crystal magnetic susceptibility measurements. For $Ni(PPh_3)_2Br_2$, HFEPR suggested $|D| = 4.5(5)$ cm$^{-1}$, $|E| = 1.5(5)$ cm$^{-1}$, $g_x = g_y = 2.2(1)$, and $g_z = 2.0(1)$, which are in agreement with concurrent magnetic measurements, but do not agree with previous single-crystal work. The previous studies were performed on a minor crystal form, while the present study was performed on the major form, and apparently the electronic parameters differ greatly between the two. HFEPR of $Ni(PPh_3)_2I_2$ was unsuccessful; however, magnetic susceptibility measurements indicated $|D| = 27.9(1)$ cm$^{-1}$, $|E| = 4.7(1)$, $g_x = 1.95(5)$, $g_y = 2.00(5)$, and $g_z = 2.11(5)$. This magnitude of the zero-field splitting (∼840 GHz) is too large for successful detection of resonances, even for current HFEPR spectrometers. The electronic structure of these complexes is discussed in terms of their molecular structure and previous electronic absorption spectroscopic studies. This analysis, which involved fitting of experimental data to ligand-field parameters, shows that the halo ligands act as strong $\pi$-donors, while the triphenylphosphane ligands are $\pi$-acceptors.

## Introduction

Standard EPR[1] spectroscopy at conventional microwave frequencies (X-band ∼9 GHz (microwave quantum energy: 0.3 cm$^{-1}$); Q-band ∼35 GHz (1.2 cm$^{-1}$)) and magnetic fields (up to ∼1.5 T) has been fruitfully employed to determine the electronic structure transition metal ions with half-integer-spin ground states (Kramers systems).[2] This method has been much less successful when applied to transition metal ions with integer-spin ground states (non-Kramers systems). In such cases, unless the symmetry about the metal ion is high (nearly cubic), the magnitude of the axial zfs parameter, $|D|$, is often larger than the available microwave quantum and the system is "EPR-silent". In high-spin integer systems with $S \geq 2$ and rhombic symmetry, some nominally spin-forbidden transitions can be detected in certain cases at frequencies much lower than $|D|$ (and usually at very low

* Author to whom correspondence should be addressed. E-mail: jtelser@roosevelt.edu.
[§] Florida State University.
[#] University of Florida.
[‡] University of Tasmania.
[†] Roosevelt University.

(1) Abbreviations used are as follows: AOM, angular overlap model; EPR, electron paramagnetic resonance; FC, field-cooled; HFEPR, high-frequency and -field EPR; HS, high-spin; LS, low-spin; S/N, signal-to-noise ratio; ZFC, zero-field cooled; zfs, zero-field splitting.

(2) Abragam, A.; Bleaney, B. *Electron Paramagnetic Resonance of Transition Ions*; Dover Publications: New York, 1986.



10.1021/ic020198j CCC: $22.00 
Published on Web 07/31/2002

magnetic fields),[2] especially when using a parallel mode detection of the EPR signal.[3,4] However, in transition metal ions with $S = 1$ ground states, such "non-Kramers" signals are not observable as they would appear at fields and/or frequencies beyond the range of conventional EPR spectrometers, even in the case of rhombic symmetry.

High-frequency and high-field EPR (HFEPR; $\nu > 90$ GHz; $B_0$ up to $\sim$25 T)[5−7] has the ability to overcome this difficulty by the combination of sufficiently high-mm/sub-mm frequencies and magnetic fields, so that EPR signals are observable in $S = 1$ systems characterized by large zfs, whether of axial or rhombic symmetry. Such an observation has been recently made for two $S = 1$ ions: $Ni^{2+}$ ($3d^8$) and $V^{3+}$ ($3d^2$), both with pseudooctahedral symmetry. In several of these HFEPR studies, the paramagnetic ions were dopants into diamagnetic hosts: $V^{3+}$ was in a $Ga^{3+}$ host with an $O_6$ donor set[8] and $Ni^{2+}$ was in a $Zn^{2+}$ host with either a $N_6$ [9] or $O_4N_2$ [10] donor set. Another study on powder $Ni^{2+}$ complexes with $N_6$ and $N_4O_2$ donor sets employed 9- and 35-GHz as well as 180-GHz HFEPR.[11]

As part of our efforts to expand the use of HFEPR in the study of "EPR-silent" molecules,[12−15] we describe here the use of this technique to study a series of solid molecular complexes of $Ni^{2+}$ in a highly distorted pseudotetrahedral environment, which produces an $S = 1$ ground state of significant zfs, and thus no observable conventional EPR spectrum.

The specific systems investigated are a series of dihalobistriphenylphosphane complexes of $Ni^{2+}$, thus having the general formula $NiL_2X_2$, where L = $PPh_3$ and X = Cl, Br, and I. The discovery of these complexes by Venzani over forty years ago was itself a significant development in inorganic chemistry.[16,17] Four-coordinate transition metal complexes of $nd^8$ electronic configuration are typically found in square-planar geometry and are thus diamagnetic ("LS $d^8$").[18] With certain, sufficiently bulky ligands, such as triphenylphosphane[16,17] and triphenylphosphane oxide,[19] $Ni^{2+}$ forms pseudotetrahedral complexes that are "HS $d^8$". The molecular and electronic structure of these complexes has been of interest for many years. Crystal structures for the series $Ni(PPh_3)_2X_2$ (X = Cl, Br, and I) were originally reported by Garton et al.[17] Much more accurate structures, which in some cases resolved crystallographic ambiguities, were subsequently reported for each of the following series: Cl,[20] Br,[21] and I.[22] Each complex clearly has pseudotetrahedral geometry, with approximately $C_{2v}$ symmetry about $Ni^{2+}$. The electronic absorption spectra of the chloro and bromo complexes have also been carefully examined,[23,24] as have their magnetic properties.[24] The study by Gerloch and coworkers is particularly noteworthy in that single-crystal magnetic susceptibility measurements were made and were combined with an analysis of the optical spectra, thereby providing a complete description of the electronic structure of $Ni(PPh_3)_2Cl_2$ and $Ni(PPh_3)_2Br_2$.[24]

Consequently, with the aim of extending the applicability of HFEPR and of providing information that complements and extends the range available by other techniques, the $Ni(PPh_3)_2X_2$ series present excellent candidates for study by HFEPR. Magnetic susceptibility measurements were also made on these complexes to provide important corroborating evidence concerning the electronic parameters determined by HFEPR. The combination of HFEPR with magnetic measurements has been useful in other studies of transition metal complexes.[25]

## Experimental Section

**Materials.** $Ni(PPh_3)_2Cl_2$ was obtained from Aldrich and used without further purification. $Ni(PPh_3)_2Br_2$ was obtained from Aldrich as well, but was also synthesized from $NiBr_2$ and $PPh_3$ in 1-butanol, as described by Venzani,[16] to give dark green needle crystals. The bulk crystalline product presumably corresponds to that crystallographically characterized,[21] synthesized using the same procedure. HFEPR results on both commercial and synthetic $Ni(PPh_3)_2Br_2$ were essentially identical. $Ni(PPh_3)_2I_2$ was synthesized following the same procedure to give dark red block crystals.

**EPR Spectroscopy.** HFEPR spectra were recorded on a spectrometer that has been previously described in detail.[26] Briefly, spectra can be recorded over the field range of 0−15 T at fundamental frequencies of 95 and 110 GHz, and at harmonic multiples of these frequencies (e.g., 190 or 220 GHz) up to the fifth harmonic (475 or 550 GHz). Mechanical tuning of the Gunn oscillator is possible within the limit of about 3 GHz above, and


(3) Hendrich, M.; Debrunner, P. *Biophys. J.* **1989**, *56*, 489−506.
(4) Campbell, K. A.; Yikilmaz, E.; Grant, C. V.; Gregor, W.; Miller, A.-F.; Britt, R. D. *J. Am. Chem. Soc.* **1999**, *121*, 4714−4715.
(5) Barra, A.-L.; Brunel, L.-C.; Gatteschi, D.; Pardi, L.; Sessoli, R. *Acc. Chem. Res.* **1998**, *31*, 460−466.
(6) Brunel, L.-C. *Physica B* **1995**, 360−362.
(7) Hagen, W. *Coord. Chem. Rev.* **1999**, *190*, 209−229.
(8) Tregenna-Piggott, P. L. W.; Weihe, H.; Bendix, J.; Barra, A.-L.; Güdel, H.-U. *Inorg. Chem.* **1999**, *38*, 5928−5929.
(9) van Dam, P. J.; Klaassen, A. A. K.; Reijerse, E. J.; Hagen, W. R. *J. Magn. Reson.* **1998**, *130*, 140−144.
(10) Pardi, L. A.; Hassan, A. K.; Hulsbergen, F. B.; Reedijk, J.; Spek, A. L.; Brunel, L.-C. *Inorg. Chem.* **2000**, *39*, 159−164.
(11) Collison, D.; Helliwell, M.; Jones, V. M.; Mabbs, F. E.; McInnes, A. J. L.; Riedi, P. C.; Smith, G. M.; Pritchard, R. G.; Cross, W. I. *J. Chem. Soc., Faraday Trans.* **1998**, *94*, 3019−3025.
(12) Goldberg, D. P.; Telser, J.; Krzystek, J.; Montalban, A. G.; Brunel, L.-C.; Barrett, A. G. M.; Hoffman, B. M. *J. Am. Chem. Soc.* **1997**, *119*, 8722−8723.
(13) Telser, J.; Pardi, L. A.; Krzystek, J.; Brunel, L.-C. *Inorg. Chem.* **1998**, *37*, 5769−5775.
(14) Krzystek, J.; Telser, J.; Pardi, L. A.; Goldberg, D. P.; Hoffman, B. M.; Brunel, L.-C. *Inorg. Chem.* **1999**, *38*, 6121−6129.
(15) Krzystek, J.; Telser, J.; Hoffman, B. M.; Brunel, L.-C.; Licoccia, S. *J. Am. Chem. Soc.* **2001**, *123*, 7890−7897.
(16) Venzani, L. M. *J. Chem. Soc.* **1958**, 719−724.
(17) Garton, G.; Henn, D. E.; Powell, H. M.; Venzani, L. M. *J. Chem. Soc.* **1963**, 3625−3629.
(18) Cotton, F. A.; Wilkinson, G.; Murillo, C. A.; Bochmann, M. In *Advanced Inorganic Chemistry*, 6th ed.; Wiley: New York, 1999; pp 840−842.
(19) Cotton, F. A.; Goodgame, D. M. L. *J. Am. Chem. Soc.* **1960**, *82*, 5771−5774.
(20) Brammer, L.; Stevens, E. D. *Acta Crystallogr.* **1989**, *C45*, 400−403.
(21) Jarvis, J. A. J.; Mais, R. H. B.; Owston, P. G. *J. Chem. Soc. (A)* **1968**, 1473−1486.
(22) Humphry, R. W.; Welch, A. J.; Welch, D. A. *Acta Crystallogr.* **1988**, *C44*, 1717−1719.
(23) Fereday, R. J.; Hathaway, B. J.; Dudley, R. J. *J. Chem. Soc. (A)* **1970**, 571−574.
(24) Davies, J. E.; Gerloch, M.; Phillips, D. J. *J. Chem. Soc., Dalton Trans.* **1979**, 1836−1842.
(25) Fanucci, G. E.; Krzystek, J.; Meisel, M. W.; Brunel, L.-C.; Talham, D. R. *J. Am. Chem. Soc.* **1998**, *120*, 5469−5479.
(26) Hassan, A. K.; Pardi, L. A.; Krzystek, J.; Sienkiewicz, A.; Goy, P.; Rohrer, M.; Brunel, L.-C. *J. Magn. Reson.* **2000**, *142*, 300−312.

below, the fundamental frequency. This tuning produces a range that increases with the harmonic number, so for example at the 5th harmonic of the 95 GHz source, the available frequency range is quite significant, amounting to ca. 460−490 GHz. Thus using the combination of available harmonics and source tuning ability provides the possibility of collecting spectra spanning a broad range of frequencies.

Typically, 30 mg of sample was used for HFEPR samples of solids. In previous HFEPR studies of pure solid samples characterized by $S = 2$, and negative $D$, magnetic field-induced torquing of microcrystallites occurred, so that quasi-single-crystal spectra were obtained at low temperatures.[12,14,15] In the $NiL_2X_2$ series, this effect was much weaker, with only partial orientation occasionally observed. These torquing effects were further prevented by the immobilization procedures used previously (embedding the sample in a KBr pellet or *n*-eicosane mull). A more frequent phenomenon in loose samples was the appearance of "pseudonoise" originating from a superposition of narrow "single-crystal-like" spectra, such as can be obtained in a simulated EPR spectrum when insufficient single-crystal orientation averaging is used.[27] We thus ground the samples before the experiment to ensure a random distribution of the crystallites in space. Even so, the high-field dispersion provided by HFEPR sometimes precluded the recording of ideal powder-pattern spectra.

**EPR Analysis.** The magnetic properties of an ion with $S = 1$ can be described by the standard spin Hamiltonian comprised of Zeeman and zfs terms:[2]

$$\mathscr{H} = \beta B \cdot \mathbf{g} \cdot S + D(S_z^2 - S(S+1)/3) + E(S_x^2 - S_y^2) \qquad (1)$$

Two different procedures were used to extract numerical values of the spin Hamiltonian parameters from the experimental spectra. In the first procedure, numerical methods were used to calculate the EPR transition energies and probabilities from the eigenvalues and eigenvectors, respectively, obtained by diagonalization of the spin Hamiltonian matrix resulting from eq 1. These results were used to create characteristic canonical resonance field versus EPR operating frequency dependencies. The program has been modified to allow nonlinear least-squares fitting (using the program DSTEPIT from QCPE, Bloomington, IN) of the spin Hamiltonian parameters to the experimental dependencies of the same kind. This procedure was used in conjunction with human judgment, which was used to eliminate unphysical, but mathematically possible, results to obtain best fit parameters for the entire field vs frequency array of EPR transitions for a given complex. As an alternative procedure, as in our previous studies, a program written by Weihe[28] was used to generate powder pattern EPR spectra for individual frequencies, ensuring the correctness of assigning the observed EPR transitions through the first procedure. Spectral simulation also aided in determining the precise resonance fields, since the experimental line shapes often did not have an ideal first derivative appearance.

**Magnetic Measurements.** Bulk magnetization measurements were obtained from a standard Quantum Design MPMS SQUID magnetometer. The samples consisted of randomly oriented microcrystals with a total mass of 170 mg for $Ni(PPh_3)_2Cl_2$, 140 mg for $Ni(PPh_3)_2Br_2$, and 100 mg for $Ni(PPh_3)_2I_2$. A small plastic can (0.273-mL polyethylene vial, Scienceware from Bel-Art Products, Pequannock, NJ) and plastic straw were used as the sample holder during the measurements. Magnetization versus temperature measurements were run from 2 to 300 K. The sample was zero-field cooled (ZFC) to 2 K before a measuring field of 0.01 or 0.1 T was applied. Data were then recorded while warming the sample from the lowest temperature. The sample was then cooled again to 2 K, but in the presence of a 0.1 T (1000 G) field, and additional field-cooled (FC) data were acquired. Magnetization versus field measurements were performed at 2 K over the field range 0−5 T.

The background signal was estimated by independently measuring a separate can and straw, and these values were subtracted from the results. The experiment uncertainty arising from the sample holder and SQUID itself contribute a maximum of $5.3 \times 10^{-4}$ emu/mol in the high-temperature region ($T \gtrsim 40$ K). The SQUID magnetometer automatically calculates an intrinsic uncertainty by using an averaging process for a measurement at a given temperature. In addition, the initial room temperature magnetization value is compared with the value recorded after the entire cool down, measurement, and warm up process is completed. This procedure provides a check on the reproducibility of the measurement and an estimate of the overall uncertainty.

The diamagnetic contribution of each sample, estimated from Pascal's constants,[29] $\chi_D = -407.4 \times 10^{-6}$ emu/mol for $Ni(PPh_3)_2Cl_2$, $-429.8 \times 10^{-6}$ emu/mol for $Ni(PPh_3)_2Br_2$, and $-461.8 \times 10^{-6}$ emu/mol for $Ni(PPh_3)_2I_2$, was then subtracted from each background corrected value to yield the paramagnetic molar susceptibility, $\chi_P$. The resulting values of the susceptibility were compared to the theoretical expectations in the high-temperature limit, i.e., near 300 K. For $Ni(PPh_3)_2Cl_2$ and $Ni(PPh_3)_2I_2$, these comparisons were in exact agreement. For $Ni(PPh_3)_2Br_2$, a direct measurement of background signal and estimated Pascal's constants corrections indicated that within the overall experimental uncertainty (see above), the resulting susceptibility agreed with the theoretical expectation in the high-temperature limit.

Magnetic susceptibility data were fit by using the same spin Hamiltonian (eq 1) and nonlinear least-squares routine as for the EPR data. Programs employed either analytical solutions to the spin Hamiltonian for an axial system[29] or exact solutions (matrix diagonalization, using the EISPACK routines) for either axial or rhombic systems. These methods have been used by some of us previously.[30,31] Analytical and exact methods gave essentially the same results for fitting to the axial case. For fits to rhombic systems, all three $g$ values were allowed to vary independently. The rhombic splitting, $E$, was either allowed to vary independently of $D$ or constrained to a magnitude $\leq D/3$. Because magnetic susceptibility data are relatively insensitive to the sign of $D$, fits were performed with $D$ constrained either to $<0$ or to $>0$, with $E$ given the same sign, where applicable. Analogous procedures were employed to fit the field-dependent magnetization data. All EPR and magnetic data fitting software are available as FORTRAN source code from the corresponding author.

**Ligand-Field Analysis.** Ligand-field parameters from the AOM model[32] were estimated for the $Ni(PPh_3)_2X_2$ complexes by using two programs in tandem: CAMMAG, written by Gerloch and coworkers,[33] and AOMX, written by Adamsky.[34] Both programs use

(27) Mombourquette, M. J.; Weil, J. A. *J. Magn. Reson.* **1992**, *99*, 37−44.
(28) Simulation software is available from Dr. H. Weihe; for more information see the WWW page: http://sophus.kiku.dk/software/epr/epr.html.
(29) O'Connor, C. J. *Prog. Inorg. Chem.* **1982**, *29*, 203−283.
(30) Telser, J.; Drago, R. S. *Inorg. Chem.* **1984**, *23*, 3114−3120.
(31) Eichhorn, D. M.; Telser, J.; Stern, C. L.; Hoffman, B. M. *Inorg. Chem.* **1994**, *33*, 3533−3537.
(32) Schäffer, C. E. *Struct. Bonding* **1968**, *5*, 68−95.
(33) Gerloch, M. *CAMMAG*, a FORTRAN program for AOM calculations; University of Cambridge: Cambridge, U.K.
(34) Adamsky, H. *AOMX*, an Angular Overlap Model Computer Program; Department of Theoretical Chemistry, Heinrich-Heine-Universität: Düsseldorf, Germany, 1994. For more information see the WWW site: http://www.theochem.uni-duesseldorf.de/~heribert/aomx/aomxhtml/aomxhtml.html.

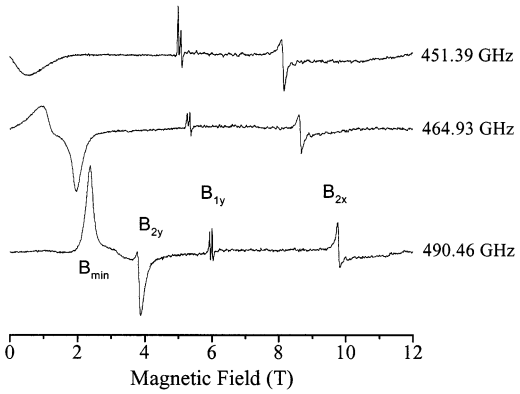


**Figure 1.** HFEPR spectra of loose $Ni(PPh_3)_2Cl_2$ at several frequencies (as indicated). Other experimental conditions: temperature, 4.5 K; field sweep rate, 0.5 T/min; field modulation frequency, 8 kHz; amplitude, 1.5 mT; available sub-mm power, ca. 10 $\mu$W. In the bottom spectrum, the specific transitions corresponding to canonical orientations in the powder pattern are identified by using the nomenclature common for triplet systems.[36]

the entire $d^n$ basis set together with geometrical information provided by X-ray structures to provide energy levels and spin and symmetry identification of d orbital states. The program AOMX allows least-squares fitting of energy levels to ligand-field parameters. Because of the local $C_{2v}$ symmetry of the $Ni(PPh_3)_2X_2$ complexes, the AOM parameters of the two triphenylphosphane ligands and of the two halo ligands were held equivalent. As in the original study by Davies et al.,[24] bonding to $PPh_3$ was described by the AOM parameters: $\epsilon\sigma$(P) and $\epsilon\pi$(P) respectively for $\sigma$- and cylindrical $\pi$-bonding, and bonding to X = Cl, Br, and I correspondingly by $\epsilon\sigma$(X) and $\epsilon\pi$(X).

## Results

**HFEPR Spectroscopy of $Ni(PPh_3)_2Cl_2$.** Typical HFEPR spectra at 4.5 K of microcrystalline $Ni(PPh_3)_2Cl_2$ at several, closely spaced, sufficiently high sub-mm wave frequencies are presented in Figure 1. The spectrum at 451.4 GHz shows a broad, but distinct zero-field signal that becomes visible in its entirety at 464.9 GHz and develops with increasing frequency into two distinct transitions visible at ~2.5 and ~4 T, respectively, at 490.5 GHz. Consideration of a rhombic spin triplet system,[35] which is assuredly the case for the $C_{2v}$ symmetry $NiL_2X_2$ complexes, allows identification of the lower field signal as $B_{min}$ and that at the higher field as $B_{2y}$. Here, and in the following, we are using the notation of Wasserman[36] for identifying the particular canonical orientations of the zfs tensor relative to the magnetic field. Two additional features, which are seen in the 450−490 GHz frequency range, move smoothly to higher field with increasing frequency and can be identified as the $B_{1y}$ and $B_{2x}$ transitions, respectively. The $B_{1y}$ transition has a peculiar shape with a repeatable double "spike" of very narrow signals (see Figure S1 (Supporting Information), where the spectrum was taken in a narrower field range). This structure is an artifact due to partial torquing, and has a beneficial side effect, namely that this transition is identifiable over a much wider frequency range than would otherwise be possible. An experiment on a sample embedded in *n*-eicosane mull at a somewhat lower frequency of 435 GHz is shown in Figure 2 and proves that the double-spiked shape of the $B_{1y}$ transition is an artifact. At this frequency, the two observed signals correspond to the $B_{1y}$ and $B_{2x}$ transitions. It is possible to match closely the resonant fields of the observed signals by using the powder pattern simulation program[28] with the following parameters: $|D| = 13.20$ cm$^{-1}$; $|E| = 1.85$ cm$^{-1}$; $g_x = 2.20$; $g_y = 2.17$; and $g_z = 2.20$. The zero-field signal appearing at 451.4 GHz in Figure 1 can be directly identified as the $(D + |E|)$ transition in the triplet manifold, thus yielding in a direct way $D + |E| = 15.05$ cm$^{-1}$.

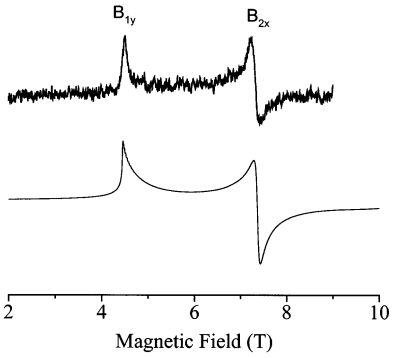


**Figure 2.** Experimental (top) and simulated (bottom) HFEPR spectra of $Ni(PPh_3)_2Cl_2$ immobilized in *n*-eicosane mull at 434.67 GHz. Other experimental conditions and identification of particular transitions are as in Figure 1. The parameters used in the simulation were the following: $D = +13.20$ cm$^{-1}$; $|E| = 1.85$ cm$^{-1}$; $g_x = 2.25$, $g_y = 2.17$, and $g_z = 2.20$; single-crystal line width, $\Delta B_x = \Delta B_z = 50$ mT, $\Delta B_y = 5$ mT.

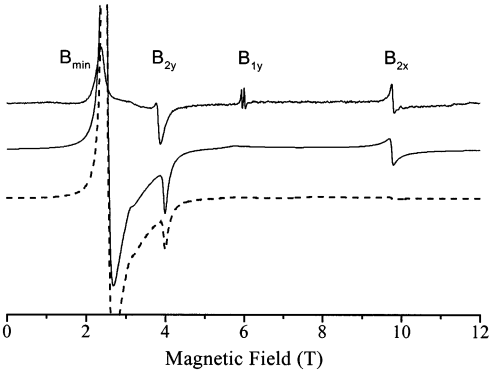


**Figure 3.** Experimental (top) and simulated (middle and bottom) HFEPR spectra of loose $Ni(PPh_3)_2Cl_2$ at 490.46 GHz and 5 K. Other experimental conditions and identification of particular transitions are as in Figure 1. The parameters used in the simulation were the following: $D = +13.20$ cm$^{-1}$ (solid line) or $D = -13.20$ cm$^{-1}$ (dashed line), $|E| = 1.85$ cm$^{-1}$; $g = 2.20$ (isotropic); and single-crystal line width, 50 mT (isotropic).

Experimental and simulated spectra at 4.5 K of $Ni(PPh_3)_2Cl_2$ at 490.46 GHz are presented in Figure 3 and corresponding spectra at 535.68 GHz are shown in Figure S2 (Supporting Information). At these highest available frequencies, corresponding to the fifth harmonic of the 95 and 110 GHz source, respectively, one finally enters the high-frequency regime ($h\nu > |D|$), resulting in powder pattern EPR spectra for $Ni(PPh_3)_2Cl_2$ more typical of triplet states.[35] At low field, $B_{min}$ is observed, and $B_{2y}$ and $B_{2x}$ are the main higher field features. Likely due to their low intensities, no *z* transitions are observed. The intensity of the $B_{min}$ transition is about 1

(35) Weltner, W., Jr. *Magnetic Atoms and Molecules*; Dover: New York, 1983.
(36) Wasserman, E.; Snyder, L. C.; Yager, W. A. *J. Chem. Phys.* **1964**, *41*, 1763−1772.

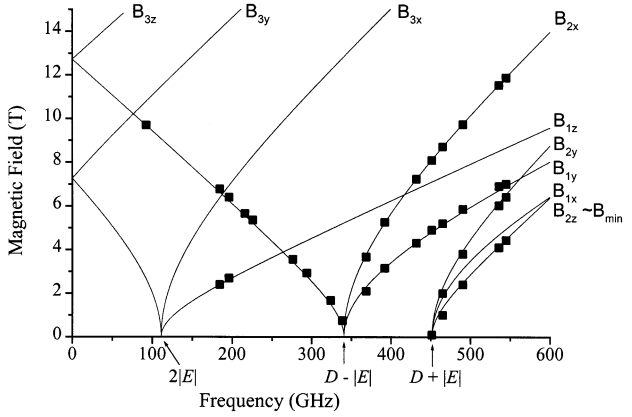


**Figure 4.** Complete resonance field vs frequency dependence of HFEPR spectra of $Ni(PPh_3)_2Cl_2$ at 5 K. Experimental resonance positions at specific frequencies are given by the squares and calculated resonances are shown by lines. Spin Hamiltonian parameters used in the calculated lines were the following: $|D| = 13.20$ cm$^{-1}$; $|E| = 1.85$ cm$^{-1}$; and $g = 2.20$ (isotropic). The calculated lines are identified by using standard nomenclature[36] for triplet states with rhombic symmetry.

order of magnitude weaker than calculated (compare simulated and experimental spectra in Figures 3 and S2), which suggests some nonrandom distribution of microcrystallites in the field due to torquing since $B_{min}$ is an off-axis turning point whose intensity strongly depends on the random distribution of crystallites in space.[36]

The entire resonance field vs frequency spectral data set of $Ni(PPh_3)_2Cl_2$, of which Figures 1−3, S1, and S2 represent cross-sections along the field axis, is shown in Figure 4. The resonances plotted in this representation form characteristic branches that are labeled according to the terminology of Wasserman.[36] Simulation of individual spectra facilitates optimal selection of resonant field values. The calculated lines through these points are based on a combination of automated nonlinear least-squares fitting with the use of human judgment to eliminate physically unreasonable results. The automated fitting procedure with isotropic $g$ led to $|D| = 13.20$ cm$^{-1}$ and $|E| = 1.85$ cm$^{-1}$, and these values provided the best fits of the individual spectra as well as of the entire 2-dimensional field-frequency data set. The fitting parameter values are summarized in Table 1. When variation in $g$ values was allowed, this procedure did lead to a slight deviation from $g_{iso} = 2.20$ (see Table 1). Although we believe that the **g** tensor is indeed likely rhombic, the level of precision warranted by the data does not allow for $g$ rhombicity to be specified and, therefore, we report the values obtained with $g_{iso} = 2.20$. This value above $g_e$ is expected for $Ni^{2+}$, a greater than half-filled d electron system.[2]

**HFEPR Spectroscopy of $Ni(PPh_3)_2Br_2$.** The HFEPR spectra for microcrystalline $Ni(PPh_3)_2Br_2$ were recorded at low temperatures, and Figure 5 presents a spectrum at 4.5 K and 325.9 GHz. The transitions in the powder spectrum are identified tentatively, as discussed below. The weak transitions marked with an asterisk (*) originate from the fourth harmonic of the fundamental frequency, which is equal to 434.5 GHz. In contrast to $Ni(PPh_3)_2Cl_2$, the $Ni(PPh_3)_2Br_2$ spectrum at this frequency strongly resembles a "typical" triplet spectrum,[35,36] with a large $B_{min}$ signal at low field and a powder pattern bounded by two features, which we assign to $B_{2y,z}$ and $B_{3y,z}$. This assignment suggests a lower magnitude of zfs in the bromo complex. The apparent noise in the spectra is not due to a low signal/noise ratio (S/N) ("actual" instrument noise), as can be seen by the excellent S/N in the $B_{min}$ region, but to signals from individual microcrystallites giving an incomplete powder pattern orientation that can be generated by computer simulation with an insufficiently fine grid.[27] This effect is even more recognizable in a spectrum taken at a somewhat lower frequency, 291 GHz, where the apparent S/N ratio again becomes very good at high field, after passing through the $B_{3y,z}$ resonance (Figure S3). Figure S3 also contains a spectrum taken at a higher frequency of 497 GHz.

The analysis of the complete set of spectra at multiple frequencies is not straightforward due to the absence of several expected transitions. Note that for the case of maximum zfs rhombicity ($|E| = |D|/3$), the $y$ and $z$ transitions ($B_{2y}$ and $B_{2z}$) overlap, and so do the two $x$ transitions ($B_{2x}$ and $B_{3x}$), which could explain the number of observed lines. The $x$ transitions come rather close to $g = 2.20$ at high frequencies, thereby making attractive its attribution to a double-quantum transition appearing in other Ni(II) systems.[9−11] At lower frequencies, however, this feature does not remain at fields corresponding to $g = 2.20$, rather it shifts to higher effective $g$ values, which is not as expected for a double-quantum transition.[9,11] An alternative attribution to some high-symmetry Ni(II) impurity with isotropic $g = 2.20$ fails for the same reason. While it is possible to simulate the spectrum in Figure 5 (326 GHz) satisfactorily (and likewise for the spectra in Figure S3), we have not found a *unique* set of values that would fully satisfactorily recreate the spectrum at *any* single frequency. Thus, no simulations are included in Figures 5 and S3.

Consequently, we have not identified a unique set of spin Hamiltonian parameters that fully model the HFEPR behavior for $Ni(PPh_3)_2Br_2$. Nevertheless, there are two viable scenarios as shown in Figure 6, which presents the complete resonance field versus frequency dependence for $Ni(PPh_3)_2Br_2$ at 4.5 K. There is a single set of experimental points (represented by squares), but two alternative sets of simulations, represented by the lines, and labeled accordingly. In Figure 6A, the following spin Hamiltonian parameters were used: $|D| = 4.5$ cm$^{-1}$; $|E| = 1.5$ cm$^{-1}$; $g_{x,y} = 2.2$; and $g_z = 2.0$. The lower simulation set, Figure 6B, used the following: $|D| = 4.2$ cm$^{-1}$; $|E| = 1.0$ cm$^{-1}$; and $g_{iso} = 2.2$.

The magnitude of $D$ is essentially the same in both cases; however, case (A) corresponds to one of maximum rhombicity, $|E| = |D|/3$, while case (B) has a lower magnitude of $E$. Only in case (A) is it possible to simulate the observed number of branches, without neglecting one or the other transition branch. Although each version shows some discrepancies between the experimental and simulated resonance field vs frequency dependencies, we believe that case (A) better reflects the reality. The discrepancies are the cause of the relatively large error margins as shown in Table 1.

**Table 1.** Electronic Parameters for $NiL_2X_2$ Complexes As Determined by Powder HFEPR and Magnetic Susceptibility Measurements

| complex | method | $D$ ($cm^{-1}$) | $\|E\|$ ($cm^{-1}$) | $g_x$ | $g_y$ | $g_z$ |
|---|---|---|---|---|---|---|
| $Ni(PPh_3)_2Cl_2$ | HFEPR[a] | +13.20(5) | 1.85(5) | 2.20(5) | 2.20(5) | 2.20(5) |
| | magnetic susceptibility, powder[a,b] | +12.03(5) | 1.78(5) | 1.99(2) | 2.00(2) | 2.40(2) |
| | magnetic susceptibility, crystal[c] | +14 | | 2.03 | | 2.51 |
| | field-dependent magnetization powder[a,d] | +13.1(2) | 0.0(2) | 2.20 (fix) | 2.20 (fix) | 2.20 (fix) |
| $Ni(PPh_3)_2Br_2$ | HFEPR[a] | +4.5(5) | 1.5(5) | 2.2(1) | 2.2(1) | 2.0(1) |
| | magnetic susceptibility, powder[a,b,e,f] | +5.38(5) | 1.76(5) | 2.06(5) | 2.00(5) | 2.22(5) |
| | magnetic susceptibility, crystal[c,e] | +13.3 | | 1.85 | | 2.77 |
| | field-dependent magnetization powder[a,d,e] | +3.8(2) | 0.0(2) | 2.00 (fix) | 2.00 (fix) | 2.00 (fix) |
| $Ni(PPh_3)_2I_2$ | magnetic susceptibility, powder[a,b] | +27.92(5) | 4.71(5) | 1.95(5) | 2.00(5) | 2.11(5) |
| | field-dependent magnetization powder[a,d] | +25.6(2) | 0.0(2) | 2.00 (fix) | 2.00 (fix) | 2.00 (fix) |

[a] This work. Values in parentheses give uncertainties. [b] Powder data over the temperature range 2−300 K at a field of 0.1 T. [c] Single-crystal data over the temperature range 20−295 K, taken from Davies et al.,[24] with powder average calculated here: $\chi_{powder} = [\chi_x + \chi_y + \chi_z]/3 = [\chi_{a^*} + \chi_b + \chi_c]/3$. Since only the magnitude of $|D|$ is important here, axial fitting was used; the single-crystal data indicated relatively small rhombic effects for both complexes. [d] Powder data over the field range 0−5 T at a temperature of 2 K. To obtain a meaningful fit, it was necessary to fix the $g$ values to those obtained from HFEPR or simply to $g = 2.00$. [e] The powder data for $Ni(PPh_3)_2Br_2$ are for the bulk crystalline form, which predominantly corresponds to that of the reported structure.[21] The single-crystal data are for a minor form, which was specifically chosen, and is described to be isomorphous with $Ni(PPh_3)_2Cl_2$, although no structure was reported.[24] [f] It was possible to fit the powder data for $Ni(PPh_3)_2Br_2$ by using a negative value for $D$ (and $E$): $D = -8.10$ $cm^{-1}$, $E = -1.60$ $cm^{-1}$, $g_x = 2.38$, $g_y = 1.89$, and $g_z = 2.03$. These magnitudes of $D$ and $E/D$ for this fit do not correspond to those from HFEPR. In particular, an absence of detectable low-field EPR transitions in the $|D| + |E| \sim 300$ GHz frequency region makes these values improbable.

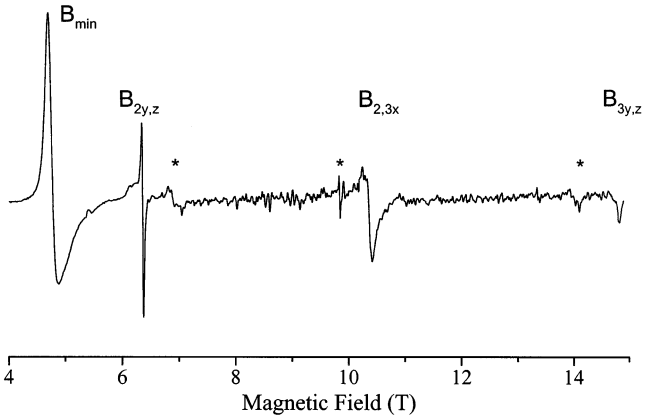


**Figure 5.** EPR spectrum of loose $Ni(PPh_3)_2Br_2$ at 325.9 GHz and 4.5 K. Other experimental conditions are as in Figure 1 with the exception of available sub-mm power, which at the third harmonic of the fundamental frequency is on the order of 1 mW. The transitions in the powder spectrum are identified and labeled tentatively, following the analysis presented in Figure 6A. The weak transitions marked with an asterisk (*) originate from the fourth harmonic, which occurs at 434.5 GHz.

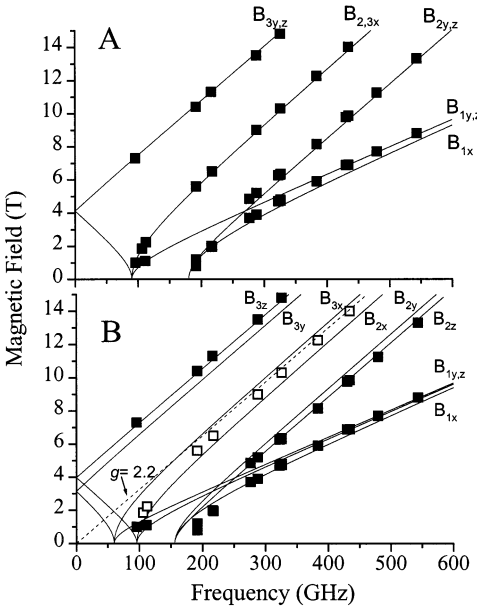


**Figure 6.** Complete resonance field vs frequency dependence of HFEPR spectra of $Ni(PPh_3)_2Br_2$ at 4.5 K. There is one set of experimental points (represented by squares) in both plots, but two alternative sets of simulations (A and B), represented by lines, and labeled accordingly. Simulation A assumed perfectly rhombic symmetry with the following spin Hamiltonian parameters: $|D| = 4.5$ $cm^{-1}$; $|E| = 1.5$ $cm^{-1}$; $g_{x,y} = 2.20$; and $g_z = 2.00$. Simulation set B used the following parameters: $|D| = 4.2$ $cm^{-1}$; $|E| = 1.0$ $cm^{-1}$; and $g = 2.20$ (isotropic). In spectrum B, the open squares represent a tentative assignment to a double-quantum transition with $g \sim 2.2$ rather than to the transition $B_{2,3x}$ (see text).

**HFEPR Spectroscopy of $Ni(PPh_3)_2I_2$.** No signals whatsoever were observed for microcrystalline $Ni(PPh_3)_2I_2$ over the entire field/frequency range available, and in the temperature range of 4.5−20 K.

**Magnetic Susceptibility Measurements of $Ni(PPh_3)_2Cl_2$, $Ni(PPh_3)_2Br_2$, and $Ni(PPh_3)_2I_2$.** Magnetic susceptibility measurements were made over the temperature range 2−300 K at fields of 0.01 and 0.1 T on microcrystalline samples of each of the three compounds of interest. Figure 7 presents these experimental data in the form of effective magnetic moment ($\mu_{eff}$) versus temperature together with a best fit line in each case. At high temperatures, for each of the three complexes $\mu_{eff} = g[S(S+1)]^{1/2} = 2.8-3.0$, exactly as expected for $S = 1$ with $g$ in the range ~2.0−2.2, consistent with the $g$ values from EPR. The high-temperature behavior of these systems is thus that of simple, mononuclear paramagnets. Qualitatively, the observed decrease in $\mu_{eff}$ at low temperature from these high-temperature, spin-only values is indicative of zfs effects.[29]

Quantitatively, magnetic susceptibility data for $Ni(PPh_3)_2Cl_2$ were well fit over the entire temperature range to an $S = 1$ system with $D = +12.03$ $cm^{-1}$, $|E| = 1.78$ $cm^{-1}$, $g_x = 1.99$, $g_y = 2.00$, and $g_z = 2.40$. Fits to an axial system ($E = 0$, $g_x \equiv g_y$) were acceptable and gave essentially the same values for $D$ and $g$, but allowance of rhombic symmetry greatly improved the fit and is more physically meaningful in this system. These fit parameters are in good agreement with those obtained by HFEPR. The variation in $g$ values is not significant, as the average $g$ value (2.13) is close to that obtained from HFEPR and, more importantly, the value for $D$ agrees to within 10%. The parameters obtained by HFEPR are likely more accurate, as they derive from simulation of resonant transitions, but there is clearly a consistent picture

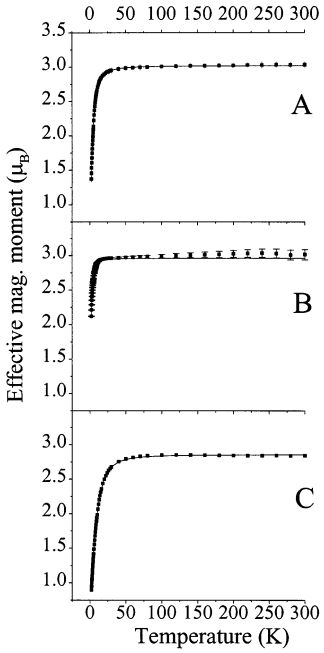


**Figure 7.** Plots of effective magnetic moment ($\mu_{eff}$) versus temperature for the three $Ni(PPh_3)_2X_2$ complexes discussed in this work. The applied field was 0.1 T. Squares represent experimental points while lines were drawn with the following spin-Hamiltonian parameters: (a) $Ni(PPh_3)_2Cl_2$, $D = +12.03$ cm$^{-1}$, $|E| = 1.78$ cm$^{-1}$, $g_x = 1.99$, $g_y = 2.00$, and $g_z = 2.40$; (b) $Ni(PPh_3)_2Br_2$, $D = +5.38$ cm$^{-1}$, $|E| = 1.76$ cm$^{-1}$, $g_x = 2.06$, $g_y = 2.00$, and $g_z = 2.22$; and (c) $Ni(PPh_3)_2I_2$, $D = +27.92$ cm$^{-1}$, $|E| = 4.71$ cm$^{-1}$, $g_x = 1.95$, $g_y = 2.00$, and $g_z = 2.11$. Error bars, determined as described in the Experimental Section, are included for all three complexes but are smaller than the symbol size for $Ni(PPh_3)_2Cl_2$ and $Ni(PPh_3)_2I_2$.

of the spin Hamiltonian parameters for $Ni(PPh_3)_2Cl_2$ based on the two techniques.

As was the case with HFEPR, the situation for $Ni(PPh_3)_2Br_2$ regarding magnetic susceptibility data is not so straightforward. It was possible to fit the observed data quite well by using a negative $D$ (ca. $-8$ cm$^{-1}$; see Table 1), but the magnitudes of both $D$ and $E/D$ are too large and too small, respectively, to be consistent with HFEPR data. Fits constrained to a positive $D$ were somewhat more problematic in that the magnitude of $E$ was increased above $D/3$, which simply corresponds to a reorienting of the coordinate system, and thus is merely a fitting artifact. When the constraint $E/D \leq 1/3$, with $E, D > 0$ was used, it was possible to fit the observed data, yielding the following parameters: $D = +5.38$ cm$^{-1}$, $E = +1.76$ cm$^{-1}$, $g_x = 2.06$, $g_y = 2.00$, and $g_z = 2.22$. These values are at least in rough agreement with those from HFEPR. The magnetic data favor a system with high, essentially maximum, rhombicity and a magnitude of $D$ that is comparable to that from HFEPR. The average $g$ value (2.09) is reasonably close to that from HFEPR (2.13) as well. Clearly, neither the magnetic nor HFEPR data provide a description of $Ni(PPh_3)_2Br_2$ that is as satisfying as for $Ni(PPh_3)_2Cl_2$. It is nevertheless reasonable to conclude that $Ni(PPh_3)_2Br_2$ is highly rhombic with $D$ positive and about $4.5 \pm 1.0$ cm$^{-1}$, much smaller than in $Ni(PPh_3)_2Cl_2$.

The magnetic susceptibility studies for $Ni(PPh_3)_2I_2$ were the most useful, since no HFEPR spectra were obtainable for this complex. The reason for this negative result appears to come from the magnetic data, where even the qualitative appearance of the $\mu_{eff}$ versus temperature curve for this complex relative to the other two shows a much more rapid decrease in $\mu_{eff}$ as the temperature decreases (Figure 7). This behavior is the consequence of a much larger magnitude of $D$, as given by the following best fit parameters: $D = +27.92$ cm$^{-1}$, $|E| = 4.71$ cm$^{-1}$, $g_x = 1.95$, $g_y = 2.00$, and $g_z = 2.11$. This magnitude of $D$, $\sim$840 GHz, with its positive sign as in $Ni(PPh_3)_2Cl_2$, would preclude the observation of EPR signals, even at the highest frequency available to us. This situation arises because all the potentially observable transitions in the available frequency/field range in the case of positive $D$ originate from the excited spin sublevels ($M_S = \pm 1$), which are only negligibly populated at low temperatures given the magnitude of $|D|$.

Last, an interesting feature of the temperature-dependent magnetization of $Ni(PPh_3)_2I_2$ was observed below 4 K, which behavior was not present in the other systems (see Figure S4). Briefly stated, we observed the zero-field cooled (ZFC) magnetization signals to be time dependent below 4 K, possessing a relaxation toward the field-cooled (FC) values with a time constant of about 28 min. This behavior is believed to be intrinsic to the material and not an experimental artifact associated with thermal equilibrium. The observed behavior may indicate the presence of a spin glasslike transition,[37] but detailed studies were not performed at this time as the behavior is likely unrelated to the properties of the individual $Ni(PPh_3)_2I_2$ molecules.

**Field-Dependent Magnetization Measurements of $Ni(PPh_3)_2Cl_2$, $Ni(PPh_3)_2Br_2$, and $Ni(PPh_3)_2I_2$.** The magnetic susceptibility measurements were performed at low fields (0.1 T) over a broad temperature range (2−300 K), while the HFEPR resonances generally occurred at fields of several T, but at low temperature ($\sim$5 K). Field-dependent magnetization measurements provide a link between these two techniques in that a bulk magnetization measurement is made, but at a single, low temperature (2 K) and over a relatively broad field range (0−5 T).

Figure 8 presents the experimental magnetization versus applied field data for microcrystalline samples of the three compounds of interest together with a best fit line in each case. Qualitatively, it can be seen that in none of the samples is saturation magnetization reached at the maximum field of 5 T. However, for $Ni(PPh_3)_2Br_2$ (Figure 8B) for which the magnitude of $D$ is smallest, the magnetization curve is the closest to achieving saturation, while for $Ni(PPh_3)_2I_2$ (Figure 8C), with the largest $D$, the magnetization curve shows no hint of saturation. Quantitatively, it is possible to fit each of these curves; however, the fitting procedure is complicated by the lack of a saturation magnetization value. In particular, to obtain meaningful fits it was necessary to fix the $g$ values as follows: for $Ni(PPh_3)_2Cl_2$, an isotropic $g = 2.20$, as found by HFEPR; for $Ni(PPh_3)_2Br_2$, the $g$ values from HFEPR are less reliable so an isotropic $g = 2.00$ was employed; for $Ni(PPh_3)_2I_2$, no HFEPR data are available so an isotropic $g = 2.00$ was also employed. Given these

(37) Mydosh, J. A. *Spin Glasses: An Experimental Introduction*; Taylor & Francis: London, UK, 1993.

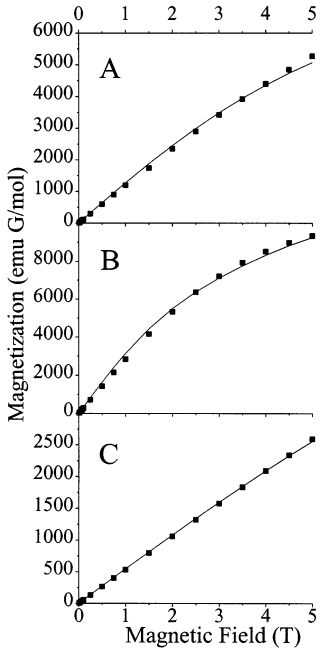


**Figure 8.** Plots of magnetization versus applied field for the three $Ni(PPh_3)_2X_2$ complexes discussed in this work. The temperature was 2 K. Squares represent experimental points while lines were drawn by using the following spin-Hamiltonian parameters: (a) $Ni(PPh_3)_2Cl_2$, $D = +13.1$ cm$^{-1}$, $E = 0.0$ cm$^{-1}$, $g_{iso} = 2.20$; (b) $Ni(PPh_3)_2Br_2$, $D = +3.82$ cm$^{-1}$, $E = 0.0$ cm$^{-1}$, and $g_{iso} = 2.00$; and (c) $Ni(PPh_3)_2I_2$, $D = +25.6$ cm$^{-1}$, $E = 0.0$ cm$^{-1}$, and $g_{iso} = 2.00$. The experimental uncertainties are less than the size of the data points.

constraints, the fits to the experimental data are quite good, as seen in Figure 8. For $Ni(PPh_3)_2Cl_2$ and $Ni(PPh_3)_2Br_2$ the resulting fit parameters are quite close to those obtained by HFEPR (see Table 1); indeed curves employing the exact parameters from HFEPR visually match the experimental magnetization data quite well (not shown). An important distinction between the HFEPR data and the field-dependent magnetization data is that the latter are almost totally insensitive to the rhombic zfs parameter, *E*. Field-dependent magnetization thus provides an important counterpart to HFEPR, but cannot provide as detailed information on electronic structure.

**Analysis of Previously Reported Magnetic Susceptibility Measurements of $Ni(PPh_3)_2Cl_2$ and $Ni(PPh_3)_2Br_2$.** Single-crystal magnetic susceptibility measurements over the temperature range 20−295 K for $Ni(PPh_3)_2Cl_2$ and $Ni(PPh_3)_2Br_2$ were performed by Davies et al.[24] They reported the molar susceptibility data for the two complexes at each of the three orthogonal principal orientations with respect to the external magnetic field.[38] For direct comparison with our powder magnetic susceptibility results, their $\chi_l$ ($l = a^*$, *b*, *c*) values at each temperature were averaged and the resulting "powder" values fit by using the same procedure as with our data. It is unfortunate that their data did not extend to lower temperature as the magnetic moment changes very little over the temperature range 20−295 K. For simplicity, therefore, only axial zfs fitting was performed. For $Ni(PPh_3)_2Cl_2$, our best fit of the single-crystal data to an axial powder model gave $|D| = 14.0$ cm$^{-1}$, $g_{x,y} = 2.03$, and $g_z = 2.51$ (fit parameters are also given in Table 1). Nevertheless, the fit was adequate and the resulting spin Hamiltonian parameters are in reasonable agreement with those obtained both by our powder susceptibility measurements and by HFEPR (see Table 1). For $Ni(PPh_3)_2Br_2$, our powder fit to their single-crystal data gave $|D| = 13.3$ cm$^{-1}$, $g_{x,y} = 1.85$, and $g_z = 2.77$. These values are in substantial disagreement with those obtained here from powder susceptibility, magnetization, and HFEPR. Possible reasons for this discrepancy will be discussed in the next section.

(38) In these complexes, the principal crystal susceptibilities (crystal axes: $a^*$, *b*, *c*) are identical with the principal molecular susceptibilities (*x*, *y*, *z*).

## Discussion

The use of high fields and frequencies has been shown to succeed in producing EPR spectra from an integer spin system that is "EPR-silent" with use of conventional methods. In $Ni(PPh_3)_2Cl_2$, a significant number of powder pattern EPR transitions were observed over a wide field range at numerous resonant frequencies. These include not only the allowed transitions, but also nominally forbidden ones, such as $B_{1y}$ in Figures 1 and 2. The axial zfs, $|D| \approx 13$ cm$^{-1}$, resulting from analysis of the two-dimensional field-frequency data set represents what we believe is a new high value in terms of what is now accessible by HFEPR. Because of the large magnitude of the zfs in this complex, it was possible to determine unequivocally the sign of *D*. Specifically, consideration of which transitions are detectable, and which are not, supports a positive sign of *D*. In particular, the $B_{3x,y}$ transitions, which are spin-allowed, are not detected in the experiment at all, even though much greater mm power is available in the 92−300 GHz range of frequencies in which they are expected to occur than in the sub-mm 330−550 GHz range where other transitions actually appear. Since these two transitions originate from a $M_S = +1$ or $-1$ spin level, these levels must be the excited levels, and the ground level is $M_S = 0$. This situation corresponds to a positive *D* in the standard representation. Additional proof is offered by spectral simulations for individual frequencies as in Figure 3.

The analysis of the powder patterns in the $Ni(PPh_3)_2Br_2$ HFEPR spectra was more complicated and hence the accuracy of the extracted spin Hamiltonian parameters was not as high as in the case of $Ni(PPh_3)_2Cl_2$. Also, the sign of *D* could not be determined. Interestingly, magnetic studies of $Ni(PPh_3)_2Br_2$ encountered similar problems. While the exact cause of these difficulties is not yet clear, one possibility is the coexistence of two or more distinct crystal structures of this complex.[24] Nevertheless, the HFEPR and magnetic data agree that $Ni(PPh_3)_2Br_2$ exhibits a strongly rhombic zfs tensor, possibly of the maximum allowed rhombicity ($|E| = |D|/3$), with zfs parameters reduced in comparison with $Ni(PPh_3)_2Cl_2$: $|D| = 4.5 \pm 0.5$ cm$^{-1}$ and $|E| = 1.5 \pm 0.5$ cm$^{-1}$. We note that in the case of $Ni(PPh_3)_2I_2$, the axial zfs determined by magnetic measurements, $|D| \approx 27$ cm$^{-1}$, is still outside the range accessible to our current HFEPR instrumentation. Planned extension of this spectro-

scopic technique into the THz range will eventually allow even such compounds to be amenable to study by EPR.

We next turn to an analysis of the spin Hamiltonian parameters obtained for each of the three complexes. As has been known for many years, the bulky triphenylphosphane ligands enforce a pseudotetrahedral geometry about $Ni^{2+}$ leading to an $S = 1$ spin ground state.[16,17] As would be expected from the steric size and differing donor abilities of the halogen versus P donor ligands, the geometry of the complexes is quite far from tetrahedral. For example, in $Ni(PPh_3)_2Cl_2$, the X−Ni−X bond angle is 128.0° (X = Cl) and the P−Ni−P bond angle is 111.4°;[20] for $Ni(PPh_3)_2Br_2$, these bond angles are 126.3° (X = Br) and 110.4°, respectively;[21] and for $Ni(PPh_3)_2I_2$, the bond angles are 118.1° (X = I) and 105.3°.[22] Using the coordinate system defined by Gerloch and co-workers,[24] the P−Ni bonds define the *xz* plane and the X−Ni bonds define the *yz* plane. The structural and bonding differences between these two sets of ligands gives rise to $C_{2v}$ rather than $D_{2d}$ symmetry, and a significant rhombic distortion about Ni, as manifest by $E \neq 0$.

The molecular structure of the $Ni(PPh_3)_2X_2$ complexes qualitatively supports the spin Hamiltonian parameters determined by HEPR. It is possible to make a more quantitative correlation by making use of other data, particularly from electronic absorption spectroscopy. This method was used in our previous study of aqueous $Cr^{2+}$,[13] which parametrized the metal ion's ligand field with use of the parameters defined by Ballhausen.[39] A similar crystal-field method was used by Gerloch and Slade in their early studies of tetrahedral $Ni^{2+}$.[40] Subsequently, Gerloch and co-workers employed the angular overlap model (AOM)[32,41] in their magnetic and spectroscopic studies of these complexes.[24,42] The AOM method has also been used by McGarvey in developing the theory of paramagnetic NMR of pseudotetrahedral complexes of $Ni^{2+}$ and $Co^{2+}$ with $D_{2d}$ point-group symmetry.[43] Because of the previous applications of AOM to pseudotetrahedral complexes of $Ni^{2+}$, we employ it here as well. Recent HFEPR studies on other integer-spin transition metal complexes have also employed AOM to analyze spin Hamiltonian parameters.[8,44]

For illustrative purposes, we show in Figure 9 the $3d^8$ triplet state energy levels of a $Ni^{2+}$ free ion with successive application of a tetrahedral and of a rhombically distorted ligand field, as found for $Ni(PPh_3)_2Cl_2$. The electronic transitions for this complex, as determined by single-crystal optical spectroscopy,[23] are specifically indicated in the figure and are roughly to scale.

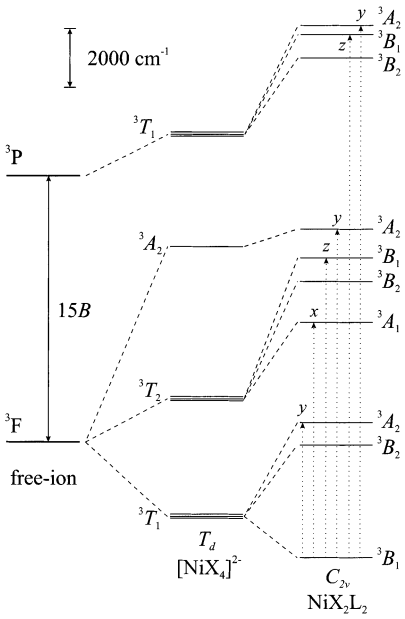


**Figure 9.** Energy levels of triplet states of $Ni^{2+}$ $3d^8$ as a free-ion, in a tetrahedral ($T_d$) ligand-field (hypothetical $[NiL_4]^{2+}$ or $[NiX_4]^{2-}$ complex), and in a rhombic ($C_{2v}$) ligand-field (actual $NiL_2X_2$ complex). The energy level spacings of the free-ion and $T_d$ cases are approximate, but those of the $C_{2v}$ case are as observed by single-crystal electronic absorption spectroscopy of $Ni(PPh_3)_3Cl_2$.[23] These electronic transitions are also indicated, together with their polarization. The state labeled $^3A_1$ also includes singlet states of similar energy. There are no symmetry-allowed transitions from the $^3B_1$ ground state to excited states of $^3B_2$ symmetry; the energy levels of these states are determined by calculation (see text). Inclusion of spin−orbit coupling with singlet states (not shown) would split each of the triplets into three nondegenerate levels, affording the rhombic zfs seen by HFEPR.

The analysis of the electronic structure of $Ni(PPh_3)_2Cl_2$ by Davies et al.[24] was based upon their single-crystal magnetic susceptibility measurements, the electronic absorption spectra reported by Fereday et al.,[23] and structural information from the original X-ray crystallographic study.[17] The crystal structure of $Ni(PPh_3)_2Cl_2$ has since been redetermined with much greater precision[20] and we have used these recent structural data in our analysis. The combination of better structural data with our experimental results necessitated changes in the ligand-field parameters of $Ni(PPh_3)_2Cl_2$ originally proposed by Davies et al.[24] Our ligand-field results for $Ni(PPh_3)_2Cl_2$ nevertheless clearly confirm their proposal[24] that the $PPh_3$ ligands are $\sigma$-donors and $\pi$-acceptors and the halo ligands are $\sigma$-donors and $\pi$-donors.

Table 2 presents the optimal values of ligand-field parameters for the $Ni(PPh_3)_2X_2$ series resulting from our fitting procedure employing the programs CAMMAG[33] and AOMX.[34] The procedure by which these parameters were obtained is described in detail in the Supporting Information. We note here only that the optimum estimate of $\epsilon\pi$(Cl) is very large (2421(29) $cm^{-1}$). However, the electronic transition energies for $Ni(PPh_3)_2Cl_2$ can be fitted almost as well (see Table S1, Supporting Information) if this parameter is constrained to a value similar to that in other complexes, although this causes the rhombic component of the zfs tensor to be considerably larger than is observed experimentally (Table 2).

(39) Ballhausen, C. J. In *Introduction to Ligand Field Theory*; McGraw-Hill: New York, 1962; pp 99−103.
(40) Gerloch, M.; Slade, R. C. *J. Chem. Soc. (A)* **1969**, 1012−1022.
(41) Figgis, B. N.; Hitchman, M. A. *Ligand Field Theory and its Applications*; Wiley-VCH: New York, 2000. See Chapter 3 and references therein for a discussion of the chemical significance of AOM parameters. See p 110 for free-ion Racah and spin−orbit coupling parameters.
(42) Gerloch, M.; McMeeking, R. F. *J. Chem. Soc., Dalton Trans.* **1975**, 2443−2451.
(43) McGarvey, B. R. *Inorg. Chem.* **1995**, *34*, 6000−6007.
(44) Barra, A.-L.; Gatteschi, D.; Sessoli, R.; Abbati, G. L.; Cornia, A.; Fabretti, A. C.; Uytterhoeven, M. G. *Angew. Chem., Int. Ed. Engl.* **1997**, *36*, 2329−2331.

**Table 2.** Ligand-Field Parameters (in $cm^{-1}$) for $Ni(PPh_3)_2X_2$ (X = Cl, Br, I) and Related Complexes

| complex | $\epsilon\sigma$(P) | $\epsilon\pi$(P) | $\epsilon\sigma$(X) | $\epsilon\pi$(X) | B | $\zeta$ |
|---|---|---|---|---|---|---|
| $Ni(PPh_3)_2Cl_2$[a,b] | 5509(43) | −1235(33) | 5227(51) | 2421(29) | 481(1) | 435(2) |
| $Ni(PPh_3)_2Cl_2$[a,c] | 4192(34) | −1674(35) | 5689(43) | 1138 | 461(1) | 347(2) |
| $Ni(PPh_3)_2Br_2$[a,d] | 4292(1351) | −501(286) | 3184(3293) | 517(3003) | 590(40) | 264(0.5) |
| $Ni(PPh_3)_2Br_2$[e] | 4000 | −1500 | 4000 | 1500 | 550 | 300 |
| $Ni(PPh_3)_2I_2$[a,f] | 5509 | −1235 | 2000 | 600 | 481 | 550 |
| $[Ni(PPh_3)Br_3]^-$ [g] | 5000 | −1500 | 3000 | 700 | 620 | |
| $[Ni(PPh_3)I_3]^-$ [g] | 6000 | −1500 | 2000 | 600 | 490 | |

[a] This work; standard deviations from fits are given in parentheses. All fits used the following relationship between the Racah parameters: $C = 4.7B$.[41] [b] Parameters determined by using recent crystallographic data[20] and by analysis of HFEPR and magnetic measurements and previous electronic absorption data. These parameters yield the following zfs: $D = +13.2$, $|E| = 1.8$ $cm^{-1}$. [c] In this case, the constraint $\epsilon\sigma(Cl)/\epsilon\pi(Cl) = 5$ was imposed (see Supporting Information). These parameters yield the following zfs: $D = +12.6$, $|E| = 3.6$ $cm^{-1}$. [d] Results for major, crystallographically characterized[21] form. Parameters determined by analysis of HFEPR and magnetic measurements and previous electronic absorption data. These parameters yield the following zfs: $D = +7.1$, $|E| = 1.4$ $cm^{-1}$. [e] Parameters reported by Davies et al. for the minor form reported to be isomorphous with $Ni(PPh_3)_2Cl_2$.[24] Use of the crystallographic data for the major form with these parameters yields the following zfs: $D = +7.6$, $|E| = 0.5$ $cm^{-1}$. [f] Parameters determined by using crystallographic data[22] and by analysis of HFEPR and magnetic measurements and correspondence with values determined for other entries in the table (see text). These parameters yield the following zfs: $D = +23.9$, $|E| = 5.8$ $cm^{-1}$. Standard deviations are not meaningful as there are no electronic absorption data to fit. [g] Parameters reported by Gerloch and Hanton.[45]

For $Ni(PPh_3)_2Br_2$, we employed structural data for the more abundant form,[21] rather than the form isomorphous with $Ni(PPh_3)_2Cl_2$.[24] The bromo complex also lacks high-quality electronic absorption data. Use of these structural data[21] and our magnetic and HFEPR data, as described in the Supporting Information, made it possible to obtain very rough estimates for the ligand-field parameters for this complex (see Table 2). This analysis reproduces the rhombic zfs observed by HFEPR and suggests a reduction in spin−orbit coupling relative to the chloro complex, which may result from increased covalency in the bromo versus the chloro complex. In the case of $Ni(PPh_3)_2I_2$, only structural[22] and our magnetic data are available. As described in the Supporting Information, use of data for a related iodo complex[45] combined with our results for $Ni(PPh_3)_2Cl_2$ allow estimates as to ligand-field parameters that provide zfs in good agreement with experiment (see Table 2). The relatively large spin−orbit coupling in this complex may be the effect of spin delocalization onto the iodo ligands.

## Conclusions

High-frequency and high-field EPR spectroscopy has been used to probe the non-Kramers, $S = 1$, $Ni^{2+}$ ion in a series of complexes of pseudotetrahedral symmetry and general formula $Ni(PPh_3)_2X_2$ (X = Cl, Br, I). For $Ni(PPh_3)_2Cl_2$, numerous EPR transitions were observed at multiple mm/sub-mm frequencies and analysis of the full, 2-dimensional field-frequency data set yielded spin Hamiltonian parameters in agreement with, but of much higher accuracy than, concurrent powder magnetic susceptibility and magnetization measurements. For $Ni(PPh_3)_2Br_2$, HFEPR spectra were again successfully recorded; however, the analysis was less conclusive. The combination of HFEPR and powder magnetic measurements (both susceptibility and field-dependent magnetization) suggests highly rhombic spin Hamiltonian parameters, with the magnitude of zfs much less than in the chloro complex (∼5 vs ∼13 $cm^{-1}$, respectively). For $Ni(PPh_3)_2I_2$, no HFEPR spectra were recorded; however, concurrent powder magnetic susceptibility and field-dependent magnetization measurements indicate a magnitude of zfs (∼27 $cm^{-1}$) that is too large too allow observation of resonances at the fields, frequencies, and temperatures employed here. The spin Hamiltonian parameters observed experimentally for $Ni(PPh_3)_2Cl_2$, in combination with previous electronic absorption data and a recent crystal structure of the complex, allowed determination of a set of electronic and bonding parameters that describe well the electronic structure of this complex. The AOM parameters for $Ni(PPh_3)_2Cl_2$ so obtained confirm previous conclusions that the phosphane ligand acts as a $\pi$-acceptor and the chloro ligand as a strong $\pi$-donor. The data for $Ni(PPh_3)_2Br_2$ do not allow unambiguous derivation of ligand field parameters, but the zfs and optical transition energies may be reproduced satisfactorily by assuming similar bonding parameters to the chloro complex, but with a significant lowering of the spin−orbit coupling due to greater covalency. In contrast, the large zfs observed for $Ni(PPh_3)_2I_2$ implies a strong spin−orbit interaction, and this may be ligand based, due to the high spin−orbit coupling constant of iodine.

**Acknowledgment.** This work was supported in part by the NHMFL (J.K. and L.-C.B.) and the Petroleum Research Fund, administered by the American Chemical Society, ACS-PRF 36163-AC5 (J.-H.P. and M.W.M.). J.T. is supported by Roosevelt University and the NHMFL User Program. We thank Prof. B. R. McGarvey, University of Windsor, Canada, for initial assistance with the ligand field analysis and Dr. H. Weihe from the Chemistry Department, University of Copenhagen, Denmark, for the simulation software and great help in implementing it. We also thank Z. X. Zhou and Dr. G. Cao, NHMFL, for initial magnetic measurements.

**Supporting Information Available:** Details of the determination of ligand-field parameters; four figures showing HFEPR spectra at different conditions and magnetization data; and a table of experimental and calculated electronic absorption data for $Ni(PPh_3)_2Cl_2$. This material is available free of charge via the Internet at http://pubs.acs.org.

(45) Gerloch, M.; Hanton, L. R. *Inorg. Chem.* **1981**, *20*, 1046−1050.

IC020198J